Wang and Cong
Journal of Engineering and Applied Science (2024) 71:73
https://doi.org/10.1186/s44147-024-00406-w

Journal of Engineering and Applied Science

RESEARCH **Open Access**

Investigation of mechanical properties of high-performance concrete via optimized neural network approaches

Xuyang Wang[1*] and Rijie Cong[2]

*Correspondence:
15144292678@163.com

[1] College of Architectural Engineering, Jilin Technology College of Electronic Information, Jilin 132021, China
[2] College of Economics and Management, Jilin Institute of Chemical Technology, Jilin 132022, China

Abstract

In this paper, an artificial intelligence approach has been employed to analyze the slump and compressive strength (CS) of high-performance concrete (HPC), focusing on its mechanical properties. The importance of assessing these critical concrete characteristics has been widely acknowledged by experts in the field, leading to the development of innovative methods for estimating parameters that typically require laboratory testing. These intelligent techniques improve the accuracy of mechanical property predictions and reduce the resource-intensive and costly nature of experimental work. The radial basis function neural network (RBFNN) is the foundational model for predicting the mechanical attributes of various HPC mixtures. To fine-tune the RBFNN's performance in replicating the mechanical properties of HPC samples, two optimization algorithms, namely the Golden Eagle Optimizer (GEO) and Dynamic Arithmetic Optimization Algorithm (DAOA), have been employed. In this manner, both RBGE and RBDA models were trained using a dataset comprising 181 HPC samples that included superplasticizers and fly ash. The results show that DAOA has significantly improved the base model's predictive capability, achieving a higher correlation with a value R^2 of 0.936 when estimating slump. Furthermore, RBDA exhibited a more favorable root mean square error (RMSE) in predicting compressive strength compared to RBGE, with a notable 16% difference. Ultimately, both integrated models demonstrated their effectiveness in accurately modeling the mechanical properties of HPC.

Keywords: Compressive strength, High-performance concrete, Slump flow, Optimization algorithm, Radial basis neural network

Introduction

Around the world, there are many more places where large-scale concrete construction is taking place. In general, related industries and businesses will be duplicated due to global trends in the construction industry towards reinforced concrete structures, the construction of tall buildings, and the development of construction techniques [1]. The safety and durability of cast concrete is a fundamental issue when using much concrete for construction. To address these issues, a lot of work has gone into developing high-performance concrete (HPC). HPC is made to offer properties that are matched to workability, strength, longevity, and durability for particular material sets, uses, and exposure conditions [2–4].

HPC can be used for structures in harsh environments, including prefabricated buildings, highways, bridges, sidewalks, and nuclear structures [5–7]. The main difference between conventional concrete and HPC is the use of particular chemical and mineral admixtures. The water content and porosity of the paste of hydrated cement will both decrease with the addition of some chemicals. It is not advisable to use high doses of chemical admixtures to reduce the water content to too low levels. The effectiveness of admixtures like superplasticizers, however, largely depends on the surrounding temperature as well as the fineness and chemistry of the cement. In place of cement, mineral admixtures can be used as pozzolanic and fine-filling materials. This strengthens and densifies the hydrated cement's microstructure. Incorporating fly ash or slag into concrete allows for a slow setting and subsequent hardening if durability is a top concern [8, 9]. Additionally, mineral mixtures are typically produced industrially, so such applications at reasonable costs can result in significant economic benefits. In light of this, it is possible to produce concrete using a superplasticizer and cement replacement materials to produce cost-effective construction materials with increased strength, workability, and durability [7, 10, 11].

Researchers have paid particular attention to determining the concrete slump flow (SL) and compressive strength (CS) factors as the mechanical properties, reflecting the quality of the materials. These procedures are primarily carried out through empirical experiments, and particular tools are used to assess the mentioned concrete features accurately. However, physical laboratory procedures are considered time-consuming and expensive, and some tools might not be available. As a result, experts are working to estimate the correlation between the SL and CS of HPC and the components of mixtures using algorithms and formulas [12–14]. Zhou et al. [15] examined the impact of aggregates on the CS of high-performance concrete. In another study, Duval and Kadri [16] examined the impact of silica-fume on compressive strength of HPC using an empirical formulations and models.

Different coefficients of regression have been produced by the experimental formulas used to evaluate the SL or CS of concretes in order to show the effects of different admixtures. As a result, the prediction processes of such formulas are uncertain, such as the relationship between the CS of concrete and highly nonlinear ingredients. Civil science fields have received highly accurate results from predictions made using artificial intelligence (AI) and machine learning (ML) techniques, particularly HPC with multiple components as opposed to traditional types. Over the past two decades, various ML algorithms with different mechanisms, such as decision trees, have been developed [7, 17]; artificial neural network (ANN) [6, 18] ensemble algorithm (EA) [19], and support vector machine (SVM) [20–22] have demonstrated that models working with ML approaches have better results compared to traditional ways in term of accuracy and time.

For predicting the ultimate strength of rectangular and square piles, Moodi et al. (2022) used ML-based techniques such as radial basis function neural network (RBNN), multi-layer perceptron (MLP), and support vector regression (SVR). The correlation index of R^2 for the MLP, RBF, and SVR procedures was calculated using experimental data from 463 samples, and it was 0.970, 0.970, and 0.91, respectively [23].

SVR technique was used by Saha et al. (2020) to identify the properties of freshly poured and hardened self-compacting concrete (SCC). The exponential radial basis function (ERBF) and RBF, two different kernel functions, were used to create the SVR model. SVR − ERBF outperformed SVR − RBF in the training and testing phases after collecting 115 experimental samples with fly ash, fine aggregate, water-powder ratio, coarse aggregate and superplasticizer, and binder content as input parameters. Results showed a correlation coefficient of 0.965, 0.954, 0.979, and 0.9773 for the predicted slump flow, L-box ratio, V-funnel, and CS, respectively [24].

In order to achieve this, the current paper aims to model the CS and SL of HPC mixtures using RBFNN. For information on feeding inputs, 181HPC samples taken from relevant literature gave information on the components of mixtures and the desired levels of CS and slump. Additionally, the main features of the RBFNN, namely the neurons, and spread, were tuned by two powerful optimization algorithms as the novelty of the current research. The algorithms that optimize these hyperparameters are Golden Eagle Optimizer (GEO) and Dynamic Arithmetic Optimization Algorithm (DAOA). Integrating RBF with GEO and DAOA enhances predictive accuracy by fitting complex patterns in concrete mix design parameters for compressive strength and slump. GEO efficiently explores the solution space, emulating golden eagles' hunting strategy. DAOA's adaptability accommodates varying concrete conditions, ensuring model effectiveness amidst changes. The approach ensures robust, generalizable predictions, reduces overfitting, and accelerates convergence, which is vital for real-time decision-making in construction. Optimal resource utilization and iterative refinement capabilities further optimize the model for maximum accuracy and efficiency.

Methods

Radial basis function neural network

The RBFNN was first presented by Broomhead and Lowe [25] and recognized as a feed-forward network trained via a supervised training algorithm. The input layer, hidden layer, and output layer are the three layers that make up the RBF, as depicted in Fig. 1. There are numerous RBF of various types, including sigmoid, polynomial, inverse poly-quadratic, and Gaussian functions. One of the useful functions given by the spread rate and center is the Gaussian type. The first section of a neural network, the input layer, contains nodes without any processes, and the number of input layer neurons equals the number of variables [26]. The hidden layer, which is the second section, resembles a calculator. In order to form the answers within the predefined curves and find the best solutions, it contains a radial function. In order to perform a nonlinear mapping of input values, the hidden layer obtains a data set from the input layer. The inputs' distance from a specific center point can be calculated using the symmetrical-based function used in this platform. With the concentrations of produced data using neurons of the hidden layer as a straightforward regression process in the output part, RBFNN on the input nodes can be applied to the output layer.

The RBF stages can be started with (a) assigning input vector (x) and the center (c_i) and their radial distance (d_i) for the nodes embedded in the hidden layer as well as

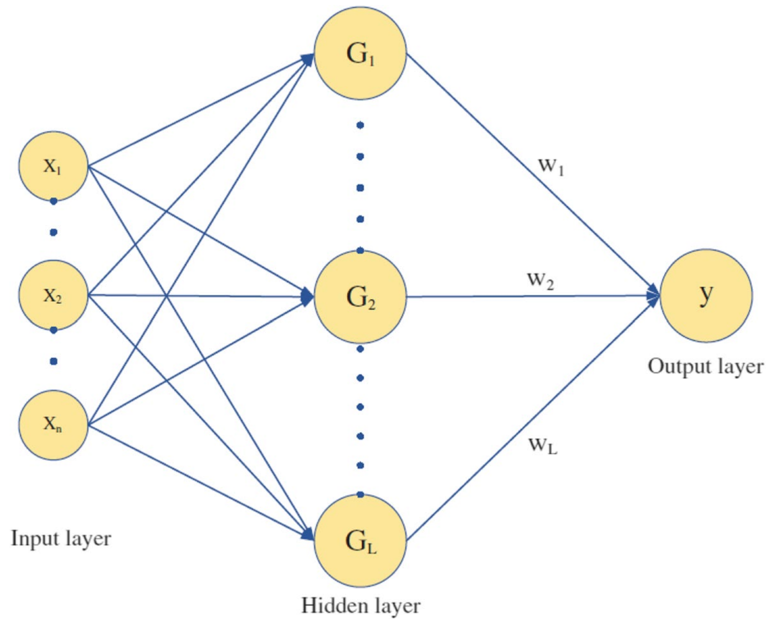

Fig. 1 Structure of RBFNN

the outcomes (h_i) appraised by the network of G using relations presented through Eqs. (1) and (2):

$$d_i = \|x - c_i\| \tag{1}$$

$$h_i = G(d_i \times \sigma_i) \tag{2}$$

where σ is the node width of the hidden layer, and G denotes the RBF. Consequently, the results can be presented using Eq. (3):

$$y = \sum_{i}^{1} w_i h_i \tag{3}$$

in which, in the hidden layer, the number of layers equals one, and w_i shows the weight among the neurons of output and hidden layers.

Dynamic arithmetic optimization

Two novel accelerator functions have been incorporated into the foundational arithmetic optimization algorithm version to enhance efficiency. The dynamic version, which controls the ratio of exploration to exploitation behavior, modifies the candidate solutions and search phase during the optimization process. What sets DAOA apart is its ability to operate without requiring any preliminary adjustments to its parameters compared to the current state-of-the-art metaheuristic. The DAOA pseudo-code is shown in Algorithm 1, while the subsequent section delves into a detailed discussion of its novel dynamic features.

Algorithm 1. Pseudo-Code of DAOA

Procedure Dynamic Arithmetic Optimization Algorithm

Initialize the Parameters for the algorithm ***α;μ***

Generate randomized values as the starting positions.

while (*t* < maximum number of iterations) ***Do***

Assess the fitness of provided solutions by calculating their values.

Identify the optimal solution.

$Update\ the\ DAF\ value\ using\ Eq.(4)$

$Update\ the\ DCS\ value\ using\ Eq.(7)$

for i D 1: $number\ of\ solutions$ $\boldsymbol{Do}$

for j D 1: $number\ of\ positions$ $\boldsymbol{Do}$

Generate random values within the range of 0 to 1 for ***r*1**, ***r*2**, ***r*3**

***if r*1** > DAF, $\boldsymbol{then\ the\ exploration\ phase}$

***if r*2** > 0:5, $\boldsymbol{then\ update\ the\ solutions'\ positions}$

$Using\ the\ first\ rule\ in\ Eq.(5)$

else

Using the second rule in Eq. (15)

end if

if r*1** < DAF, ***then the exploitation phase

if r*3** > 0:5, ***then update the solutions' positions

Using the first rule in Eq. (6)

else

Using the second rule in Eq. (6)

$\boldsymbol{end\ if}$

$\boldsymbol{end\ if}$

$\boldsymbol{end\ for}$

$\boldsymbol{end\ for}$

t D *t* C 1

end while

Provide the top-performing solution.

end procedure

Dynamic accelerated function for DAOA

The arithmetic optimization algorithm's dynamic component relies heavily on the essential role played by the dynamic accelerated function (DAF) during the search process. When using the AOA, it is necessary to fine-tune the initial min and max values of the accelerated function. However, employing an algorithm devoid of internally adjustable parameters is preferable, given that DAF is substituted with a fresh descending function. This adjustment factor in the optimization algorithm is presented as follows:

$$DAF = \left(\frac{Iter_{max}}{Iter}\right)^{\alpha} \tag{4}$$

In this context, "*Iter*"represents the ongoing iteration count, "*Itermax*", signifies the upper limit for iterations, and the value of "α" remains a constant. The function undergoes a reduction with each successive iteration within the algorithm.

Dynamic DAOA candidate solution

The following dynamic qualities created for potential solutions in the DAOA are shown in this section. There are two main stages of metaheuristic algorithms: exploration and exploitation. Achieving a balanced balance between these stages is essential to the algorithm's performance. During the optimization process, each solution in the suggested dynamic adaptation which places a high emphasis on maximizing exploration and exploitation constantly adjusts its positions by making reference to the best-obtained solution. Equation (5) in the fundamental version is replaced with Eq. (6) in the dynamic candidate solution (DCS) function.

$$x_{i,j}(C_{iter}+1) = \begin{cases} best(x_j) \div (DCS+\epsilon) \times ((UB_j - LB_j) \times \mu + LB_j)), r2 < 0.5 \\ best(x_j) \times DCS \times ((UB_j - LB_j) \times \mu + LB_j)) Otherwise \end{cases} \tag{5}$$

$$x_{i,j}(C_{iter}+1) = \begin{cases} best(x_j) - DCS \times ((UB_j - LB_j) \times \mu + LB_j)), r3 < 0.5 \\ best(x_j) + DCS \times ((UB_j) \times \mu + LB_j)), Otherwise \end{cases} \tag{6}$$

Introducing the DCS function directly responds to the decreasing proportion of candidate solutions. Its value continually reduces during each iteration, adhering to this established pattern.

$$DCS(0) = 1 - \sqrt{\frac{Iter}{Iter_{max}}} \tag{7}$$

$$DCS(t+1) = DCS(t) \times 0.99 \tag{8}$$

Golden eagle optimization

Golden eagles have a special relationship with humans, holding sacred positions in beliefs and being seen as signs of fortunate events. They hunt in Kazakhstan and Kyrgyzstan, using a unique spiral-shaped cruising and hunting motion. They balance their propensity to cruise and attack, making extensive circles around their territory. They alert other eagles to their best catch and continue to hunt throughout the flight, using both cruising and attacking strategies.

The golden eagle's balance between exploration and exploitation is reflected in its flight pattern. A metaheuristic algorithm, GEO, is developed based on this spiraling pattern, segmenting ROD images for precise examination and disease diagnosis. Consider a hypothetical RGB image with dimensions $M * N$. The image element $(pixel)$ at (x, y) is therefore equal to:

$$F\left(x, y\right) whilex \in \{1, 2, 3, \ldots, M\} \; and \; y \in \{1, 2, 3, \ldots, N\}$$

Assuming T is the experimental image's grey level and that the overall grey values are $0, 1, 2, 3, ..., T - 1$, indicated by R, as follows:

$$F\left(x, y\right) \in R^{\forall}(x, y) \in picture \tag{9}$$

The following is the definition of the image's standardized histogram (bar chart):

$$J = \{j0.j1, \ldots jR1\} \tag{10}$$

The equation above can be expressed as follows using the geometrically active multi-contours method:

$$J(Th) = j0(th_1) + j1(th_2), \ldots, jR - 1\left(th_{k-1}\right) \tag{11}$$

$$Th* = \max\{J(Th)\} \tag{12}$$

$Th*$ stands for the threshold of choice. The GEO technique uses the DRLS method to extract data from preprocessed images, requiring fewer initial parameters. The data is normalized, used as training data for a vector machine model, and compared to expert observational images. The first step involves calculating image similarity metrics like GEOccard, Dice, FPR, and FNR by the articles. The mathematical formula is shown below:

$$Jaccard\left(I_g, I_m\right) = I_g \cap I_m / I_g \cup I_m \tag{13}$$

$$Dice\left(I_g, I_m\right) = 2\left(I_g \cap I_m\right) / \left|I_g\right| \cup |I_m| \tag{14}$$

$$FPR\left(I_g, I_m\right) = \left(I_g / I_m\right) / \left(I_g \cup I_m\right) \tag{15}$$

$$FNR\left(I_g, I_m\right) = \left(I_m / I_g\right) / \left(I_g \cup I_m\right) \tag{16}$$

Additionally, the following formulas are used to calculate the image's statistical values, including sensitivity, specificity, and accuracy:

$$Sensitivity = \frac{T_P}{(T_P + F_N)} \tag{17}$$

$$Specificity = \frac{T_N}{(T_N + F_P)} \tag{18}$$

$$Accuracy = \frac{(T_P + T_N)}{(T_P + T_N + F_P + F_N)} \tag{19}$$

T_N, T_P, F_N, and F_P stand for true negative, true positive, false negative, and false positive, respectively. I_g is equal to GT. I_m is the extracted region.

Data gathering

The current study uses an experimental data set including 181HPC mixes [27] with constituents: ratio of water to binder, fine aggregates to coarse aggregates ratio, fly ash, air entraining agent, and additive of superplasticizer which Fig. 2 has indicated symbol-line plot for the input and output. It is important to remember that the SL and CS measured magnitudes were performed on concrete that was 28 days old. Table 1 provides a general summary of the inputs to the models, including constituents (state variables) and geotechnical characteristics of CS and slump flow.

Assessing the developed hybrid models

Several metrics have been used to investigate the RBDA and RBEO performance to estimate the slump and CS rates of HPC mixes; they are introduced in Eqs. (20) through (24), where p_n represents predicted values and t_n represents measured values, and N represents the number of samples. Also, n_{train} and n_{test} represent the number of concrete compounds for the training and testing steps, respectively.

$$MAE = \frac{1}{N}\sum_{n=1}^{N}|p_n - t_n| \tag{20}$$

$$VAF = \left(1 - \frac{var(p_n - t_n)}{var(t_n)}\right) * 100 \tag{21}$$

$$RMSE = \sqrt{\frac{1}{N}\sum_{n=1}^{N}(p_n - t_n)^2} \tag{22}$$

$$OBJ = \left(\frac{n_{train} - n_{test}}{n_{train} + n_{test}}\right)\frac{RMSE_{train} + MAE_{test}}{R^2_{train} + 1} + \left(\frac{2n_{train}}{n_{train} + n_{test}}\right)\frac{RMSE_{test} - MAE_{test}}{R^2_{test} + 1} \tag{23}$$

$$R^2 = \left(\frac{\sum_{n=1}^{N}\left(t_n - \overline{t}\right)(p_n - \overline{p})}{\sqrt{\left[\sum_{n=1}^{N}(t_n - \overline{p})^2\right]\left[\sum_{n=1}^{N}(p_n - \overline{p})^2\right]}}\right)^2 \tag{24}$$

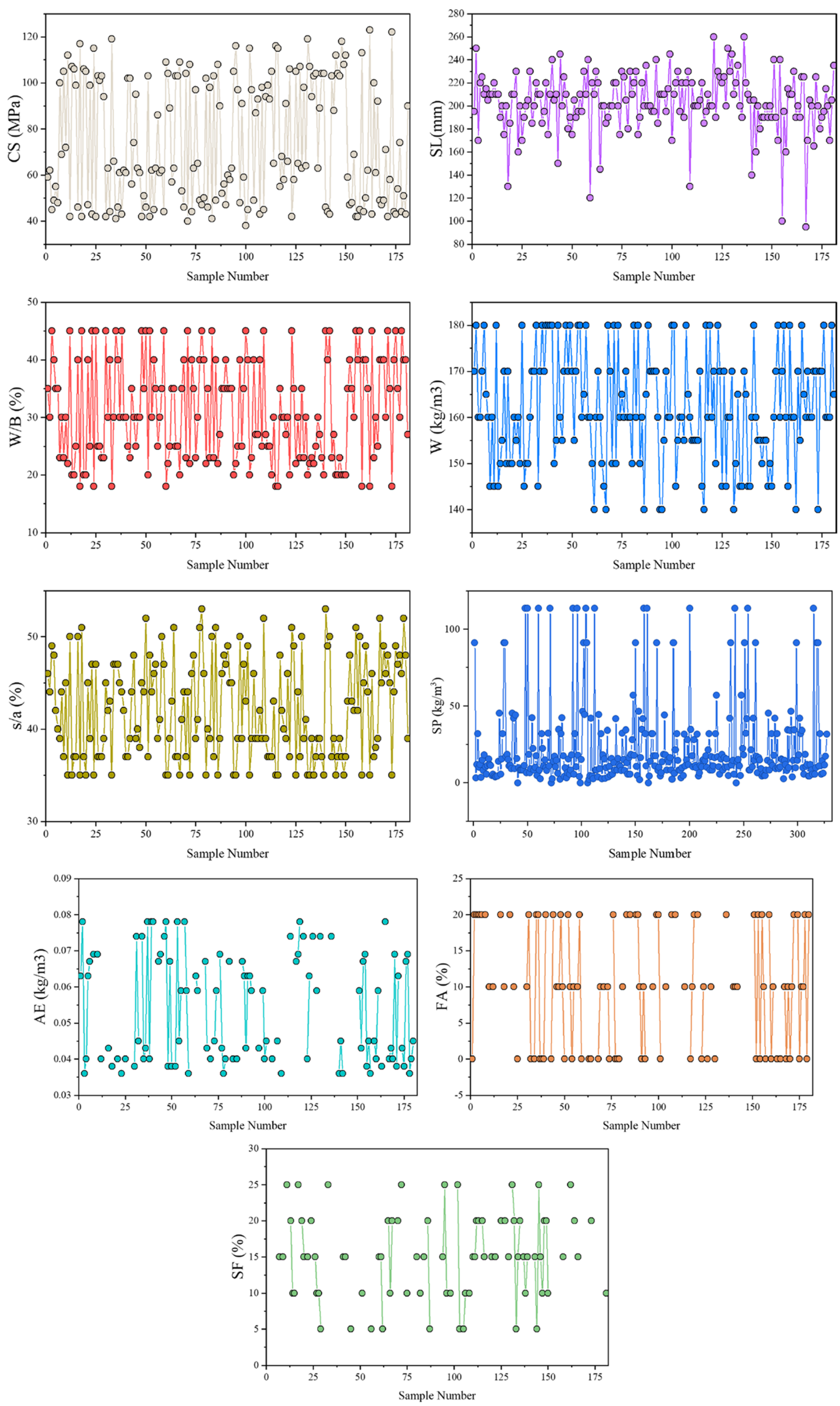

Fig. 2 Line symbol plot for the input and output

Table 1 Summary statistical report of model inputs

Parameter	Unit	Code	Max	Min	Ave	St. Dev
Compressive strength	(MPa)	CS	123	38	74.17	26.64
Slump flow	(mm)	SL	260	95	202.73	25.93
Water/binder	(%)	W/B	45	18	31.17	8.77
Water	(kg/m^3)	W	180	140	162.13	12.12
Fine aggregates/all aggregates	(%)	S/A	53	35	42.15	5.37
Fly ash	(%)	FA	20	0	5.8	8.03
Air entraining agent	(kg/m^3)	AE	0.08	0	0.03	0.03
Silica-fume	(%)	SF	25	0	6.44	8.43
Superplasticizer	(kg/m^3)	SP	36.5	1.89	10.93	8.63

Table 2 The result of developed models for RBF

HPC feature	Model	Phase	Index values				
			R^2	RMSE	MAE	VAF	OBJ
Compressive strength	RBGE	Train	0.911	9.222	8.602	98.64	-
		Test	0.898	8.506	7.003	96.70	-
		All	0.896	8.551	7.234	97.51	7.13
	RBDA	Train	0.928	7.932	6.024	96.73	-
		Test	0.922	7.411	6.165	97.61	-
		All	0.923	7.380	6.070	97.51	8.64
Slump flow	RBGE	Train	0.911	9.222	8.602	98.64	-
		Test	0.915	8.504	6.988	97.23	-
		All	0.909	8.549	7.223	97.79	7.08
	RBDA	Train	0.928	7.932	6.024	97.28	-
		Test	0.936	7.382	6.112	97.97	-
		All	0.933	7.360	6.03	97.79	8.59

Here, t_n shows the measured numbers of CS and SL, and the means are indicated via $\overline{t}$; the estimated values have been indicated with p_n with mean of $\overline{p}$. The number of HPC mixtures for the training and testing phases is shown by n_{train} and n_{test}, alternatively.

Results and discussions

The primary objectives of the current study revolved around modeling the mechanical properties of HPC samples. By integrating the optimization techniques employed in this research with the RBFNN model, two distinct models known as RBDA and RBGE were developed, showcasing their ability to predict the CS and SL of HPC mixtures with remarkable accuracy. Both models underwent comprehensive evaluation in terms of their performance in predicting CS and SL from multiple perspectives. Table 2 presents the results of developed models using the RBF to predict CS and HPC slump. The table comprises evaluation metrics such as R^2, RMSE, MAE, VAF, and OBJ. The HPC features differentiate the models, the specific RBF-based model (RBGE or RBDA), and the evaluation phase (train, test, or all, denoting a combined evaluation).

RBGE and RBDA models are evaluated in the training and testing phases to predict CS. In the training phase, RBDA demonstrates a higher R^2 (0.928) than RBGE (0.911), indicating better accuracy. In the testing phase, RBDA maintains a slightly higher R^2 (0.922) and lower RMSE (7.411) compared to RBGE ($R^2 = 0.898$, RMSE = 8.506). Overall, considering all data, RBDA consistently shows a marginally superior R^2 (0.923) and lower RMSE (7.380) compared to RBGE ($R^2 = 0.896$, RMSE = 8.551). Additionally, the OBJ values for RBDA in the combined evaluation are 8.64, suggesting optimization efficiency.

Similarly, RBGE and RBDA models undergo evaluation in the training and testing phases for predicting slump flow. RBDA exhibits a slightly higher R^2 and lower RMSE than RBGE across the training, testing, and combined datasets. Notably, in the testing phase, RBDA achieves a higher R^2 (0.936) and lower RMSE (7.382) compared to RBGE ($R^2 = 0.915$, RMSE = 8.504). The overall evaluation reiterates RBDA's marginally superior performance, with a higher R^2 (0.933) and lower RMSE (7.360) compared to RBGE ($R^2 = 0.909$, RMSE = 8.549). The OBJ values for RBDA in the combined evaluation are 8.59, indicating efficient optimization. These results demonstrate that RBDA exhibits slightly better accuracy and lower error metrics than RBGE in predicting CS and slump.

Figure 3 illustrates the relationship between observed and projected CS and SL values in HPC using data points. It compares two models: RBDA, which combines an RBF model with DAOA optimization, and RBGE, which pairs an RBF model with GEO optimization, for predicting CS and SL values. The graph includes an R^2 evaluation, positioning training, validation, and testing data points around a central reference line

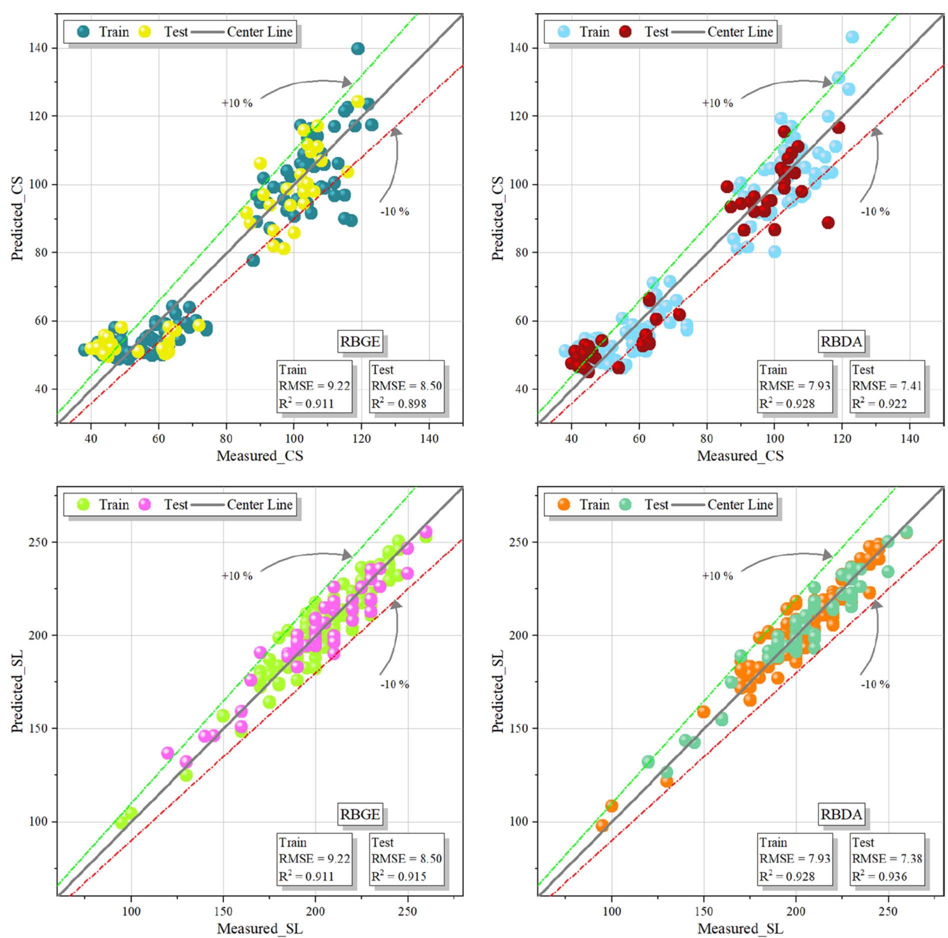

Fig. 3 Correlation between the measured and predicted values

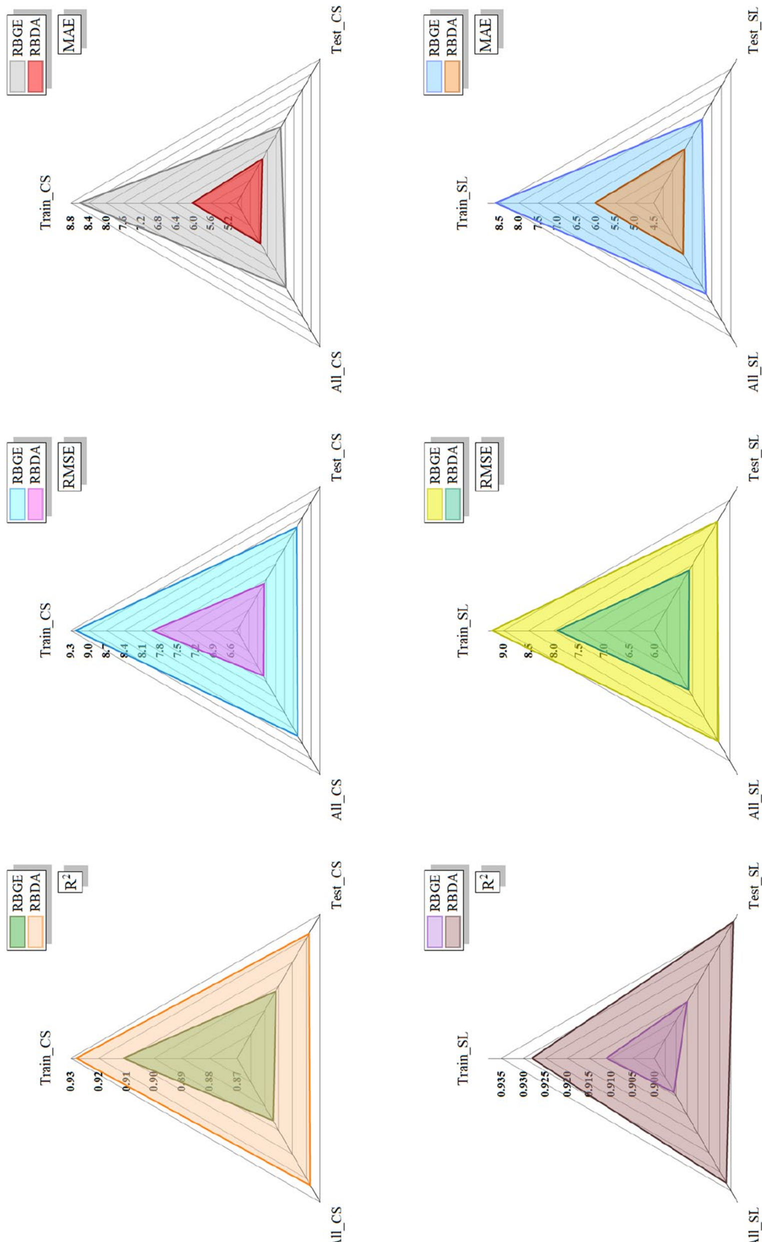

Fig. 4 Comparison for the developed models is based on metrics

($Y = X$) for linear regression. Two boundary lines ($Y = 0.9X$ and $Y = 1.1X$) indicate potential deviations from the central line, highlighting possible accuracy issues. The analysis shows that the RBDA hybrid model consistently outperforms the RBGE model in terms of R^2 and RMSE, especially in the training phase for CS prediction and the testing phase for SL prediction.

The additional examination of Fig. 4, which contrasts the R^2, RMSE, and MAE metrics of different models, strengthens the observation that the RBDA hybrid model's predictions closely align with the actual test outcomes. Within the context of this figure, a notable trend can be observed: the lines connecting the R^2 values of the RBDA across three distinct phases are positioned near the edges of the triangle. In sharp contrast, the lines representing the error values of the RBDA for these phases are clustered in the central area of the triangle. This particular distribution pattern serves as a compelling signal of the model's impressive precision.

In Figs. 5 and 6, the error percentages for CS and SL prediction in HPC are depicted in radial and line plots for both the RBGE and RBDA models. In the CS plots, maximum errors are recorded as approximately (−0.25, 0.35) during the testing phase and (−0.2, 0.3) in the training phase for the RBGE model. As for the SL plots, maximum errors of approximately (−0.2, 0.35) during the testing phase and (−0.25, 0.22) in the training phase are observed for the RBGE model.

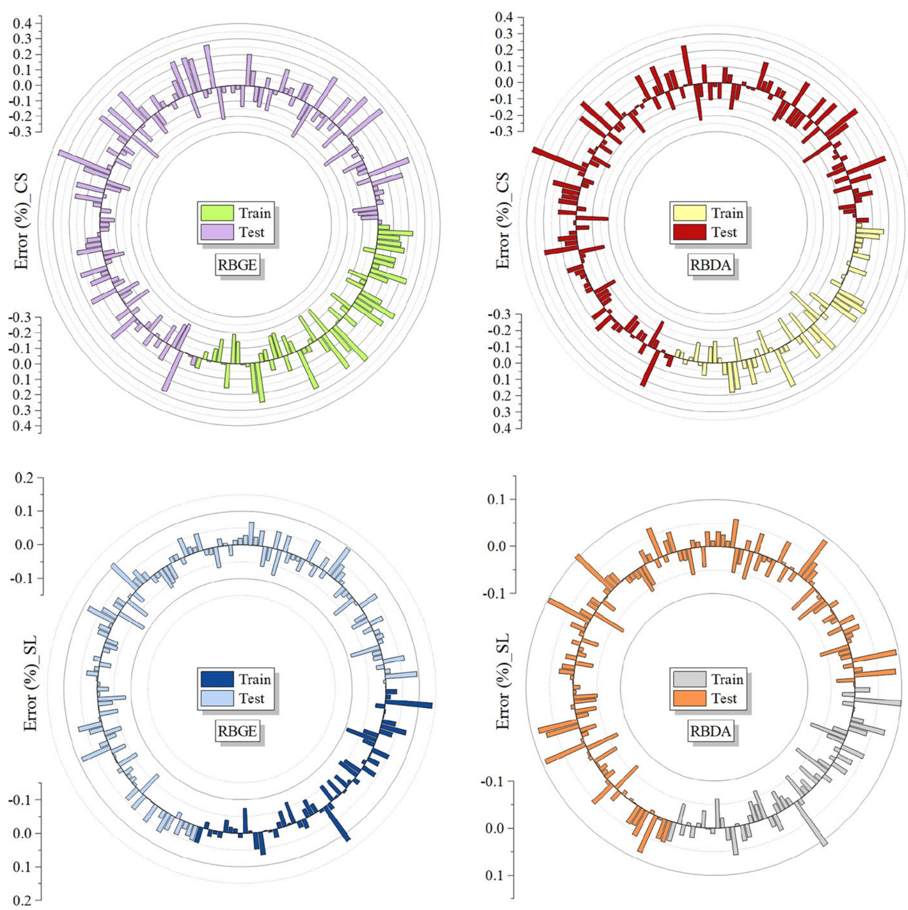

Fig. 5 The error percentage for the hybrid models is based on the radial plot

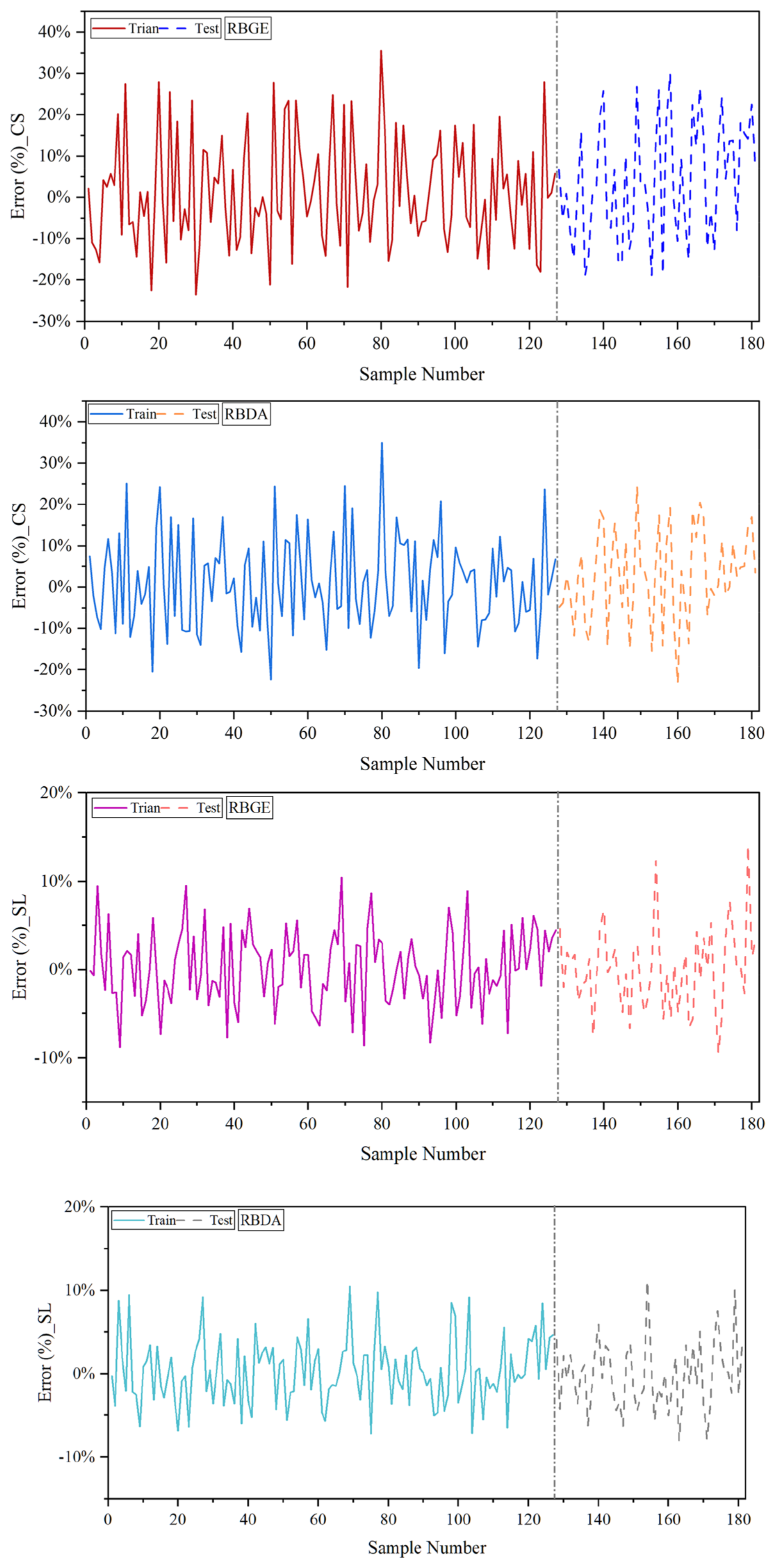

Fig. 6 The line plot of errors among the developed models

Conclusions

This paper employs an artificial intelligence approach to model the SL and CS of HPC, focusing on their mechanical properties. Recognizing the significance of accurately estimating these crucial concrete characteristics, experts have emphasized the need for novel, more efficient procedures that reduce reliance on laboratory experiments. These intelligent methods can enhance the precision of mechanical property predictions and reduce the associated physical energy and experimental costs. In this pursuit, the RBFNN is the foundational model for predicting the mechanical properties of HPC mixtures. Furthermore, two optimization algorithms, namely the GEO and the DAOA, are employed to fine-tune the RBFNN's operations in replicating the mechanical properties, specifically CS and SL, of HPC samples. The results obtained from both models in predicting CS and SL are similar, but the performance of the DAOA optimizer is demonstrated to be superior when coupled with the RBFNN. For instance, in the estimation of CS, the RBDA framework achieved an R^2 coefficient of 0.928 during the training phase, which is 2.74% higher than that of RBGE. In the testing phase, the correlation coefficients were calculated at 0.922 for RBDA and 0.898 for the other model, affirming the effectiveness of the training stage in reducing error rates. The error margins for slump predictions range from -15 to $+20\%$, while for CS, they span $\pm40\%$. Although RBDA exhibited weaker performance in the testing phase when estimating CS, error fluctuations became more pronounced during testing. However, RBDA's estimated SL values were superior to those of RBGE, with the highest errors observed in the testing phase when appraising SL and the training phase when estimating CS.

In conclusion, the results confirm the capabilities of both frameworks to simulate CS and SL, representing mechanical properties at acceptable levels. In most cases, DAOA proves to be a highly accurate optimizer for fine-tuning RBFNN compared to GEO. Utilizing such intelligent methods instead of costly experimental approaches can significantly improve the cost-effectiveness of research endeavors, especially in future studies where these models can be employed for sensitivity analyses of concrete mixture constituents.

Acknowledgements

I would like to take this opportunity to acknowledge that there are no individuals or organizations that require acknowledgment for their contributions to this work.

Authors' contributions

All authors contributed to the study conception and design. Data collection, simulation, and analysis were performed by " Xuyang Wang and Rijie Cong". The first draft of the manuscript was written by " Xuyang Wang"and all authors commented on previous versions of the manuscript. All authors have read and approved the manuscript.

Funding

This work was supported by the Jilin City Social Science Association, research on the promotion strategy of ecological livable city in Jilin City based on collaborative governance theory (Project No.: 2224).

Availability of data and materials

The authors do not have permissions to share data.

Declarations

Competing interests

The authors declare no competing interests.

Received: 26 September 2023 Accepted: 4 March 2024
Published online: 15 March 2024

References

1. Sohail MG et al (2018) Advancements in concrete mix designs: high-performance and ultrahigh-performance concretes from 1970 to 2016. J Mater Civ Eng 30(3):4017310. https://doi.org/10.1061/(ASCE)MT.1943-5533.0002144
2. Golafshani EM, Behnood A, Hosseinikebria SS, Arashpour M (2021) Novel metaheuristic-based type-2 fuzzy inference system for predicting the compressive strength of recycled aggregate concrete. J Clean Prod 320:128771
3. Cheng M-Y, Prayogo D, Wu Y-W (2014) Novel genetic algorithm-based evolutionary support vector machine for optimizing high-performance concrete mixture. J Comput Civ Eng 28(4):6014003
4. Golewski GL (2018) Green concrete composite incorporating fly ash with high strength and fracture toughness. J Clean Prod 172:218–226
5. Behnam Sedaghat, G. G. Tejani, and S. Kumar 2023 Predict the maximum dry density of soil based on individual and hybrid methods of machine learning, Adv. Eng. Intell. Syst 002, 03, https://doi.org/10.22034/aeis.2023.414188.1129.
6. S. Chithra, S. R. R. S. Kumar, K. Chinnaraju, and F. Alfin Ashmita 2016 A comparative study on the compressive strength prediction models for high performance concrete containing nano silica and copper slag using regression analysis and artificial neural networks, Constr. Build. Mater 114:528–535 https://doi.org/10.1016/j.conbuildmat.2016.03.214.
7. Farooq F et al (2020) A comparative study of random forest and genetic engineering programming for the prediction of compressive strength of high strength concrete (HSC). Appl Sci 10(20):7330. https://doi.org/10.3390/app10207330
8. Alsalman A, Dang CN, Prinz GS, Hale WM (2017) Evaluation of modulus of elasticity of ultra-high performance concrete. Constr Build Mater 153:918–928. https://doi.org/10.1016/j.conbuildmat.2017.07.158
9. Zhu Y, Zhang Y, Hussein HH, Chen G (2020) Flexural strengthening of reinforced concrete beams or slabs using ultra-high performance concrete (UHPC): a state of the art review. Eng Struct 205:110035
10. Yu K-Q, Yu J-T, Dai J-G, Lu Z-D, Shah SP (2018) Development of ultra-high performance engineered cementitious composites using polyethylene (PE) fibers. Constr Build Mater 158:217–227
11. Alkaysi M, El-Tawil S (2017) Factors affecting bond development between Ultra High Performance Concrete (UHPC) and steel bar reinforcement. Constr Build Mater 144:412–422. https://doi.org/10.1016/j.conbuildmat.2017.03.091
12. A. Khajeh, S. A. Ebrahimi, H. MolaAbasi, R. Jamshidi Chenari, and M. Payan, 2021 Effect of EPS beads in lightening a typical zeolite and cement-treated sand, Bull. Eng. Geol. Environ 80(11):8615–8632 https://doi.org/10.1007/s10064-021-02458-1.
13. Akbarzadeh MR, Ghafourian H, Anvari A, Pourhanasa R, Nehdi ML (2023) Estimating compressive strength of concrete using neural electromagnetic field optimization. Materials (Basel) 16(11):4200
14. A. Tavana Amlashi, E. Mohammadi Golafshani, S. A. Ebrahimi, and A. Behnood 2023 Estimation of the compressive strength of green concretes containing rice husk ash: a comparison of different machine learning approaches, Eur. J. Environ. Civ. Eng 27(2):961–983 https://doi.org/10.1080/19648189.2022.2068657.
15. Zhou FP, Lydon FD, Barr BIG (1995) Effect of coarse aggregate on elastic modulus and compressive strength of high performance concrete. Cem Concr Res 25(1):177–186. https://doi.org/10.1016/0008-8846(94)00125-I
16. Duval R, Kadri EH (1998) Influence of silica fume on the workability and the compressive strength of high-performance concretes. Cem Concr Res 28(4):533–547
17. Cheng M-Y, Firdausi PM, Prayogo D (2014) High-performance concrete compressive strength prediction using Genetic Weighted Pyramid Operation Tree (GWPOT). Eng Appl Artif Intell 29:104–113. https://doi.org/10.1016/j.engappai.2013.11.014
18. Bui D-K, Nguyen T, Chou J-S, Nguyen-Xuan H, Ngo TD (2018) A modified firefly algorithm-artificial neural network expert system for predicting compressive and tensile strength of high-performance concrete. Constr Build Mater 180:320–333. https://doi.org/10.1016/j.conbuildmat.2018.05.201
19. Chou J-S, Pham A-D (2013) Enhanced artificial intelligence for ensemble approach to predicting high performance concrete compressive strength. Constr Build Mater 49:554–563
20. Li E et al (2021) Developing a hybrid model of salp swarm algorithm-based support vector machine to predict the strength of fiber-reinforced cemented paste backfill. Eng Comput 37(4):3519–3540
21. Zhang S, Liu C, Wang W, Chang B (2020) Twin least square support vector regression model based on gauss-laplace mixed noise feature with its application in wind speed prediction. Entropy 22(10):1102
22. Abd AM, Abd SM (2017) Modelling the strength of lightweight foamed concrete using support vector machine (SVM). Case Stud Constr Mater 6:8–15. https://doi.org/10.1016/j.cscm.2016.11.002
23. Moodi Y, Ghasemi M, Mousavi SR (2022) Estimating the compressive strength of rectangular fiber reinforced polymer–confined columns using multilayer perceptron, radial basis function, and support vector regression methods. J Reinf Plast Compos 41(3–4):130–146
24. Saha P, Debnath P, Thomas P (2020) Prediction of fresh and hardened properties of self-compacting concrete using support vector regression approach. Neural Comput Appl 32(12):7995–8010
25. D. S. Broomhead and D. Lowe, Radial basis functions, multi-variable functional interpolation and adaptive networks, Royal Signals and Radar Establishment Malvern (United Kingdom), 1988.
26. Golafshani EM, Behnood A (2018) Application of soft computing methods for predicting the elastic modulus of recycled aggregate concrete. J Clean Prod 176:1163–1176
27. Lim C-H, Yoon Y-S, Kim J-H (2004) Genetic algorithm in mix proportioning of high-performance concrete. Cem Concr Res 34(3):409–420

Publisher's Note